

## Retrieving Bulge and Disk Parameters and Asymptotic Magnitudes from the Growth Curves of Galaxies

Sadanori Okamura, Naoki Yasuda<sup>1</sup>, Kazuhiro Shimasaku, and Masafumi Yagi<sup>1</sup>  
 Department of Astronomy and Research Center for the Early Universe, School of Science,  
 University of Tokyo, Bunkyo-ku, Tokyo, 113-0033 Japan; okamura@astron.s.u-tokyo.ac.jp

and

David H. Weinberg  
 Department of Astronomy, Ohio State University, Columbus, OH, 43210, USA;  
 dhw@astronomy.ohio-state.edu

### ABSTRACT

We show that the growth curves of galaxies can be used to determine their bulge and disk parameters and bulge-to-total luminosity ratios, in addition to their conventional asymptotic magnitudes, provided that the point spread function is accurately known and signal-to-noise ratio is modest ( $S/N \gtrsim 30$ ). The growth curve is a fundamental quantity that most future large galaxy imaging surveys will measure. Bulge and disk parameters retrieved from the growth curve will enable us to perform statistical studies of luminosity structure for a large number of galaxies.

*Subject headings:* galaxies: photometry, growth curve, bulge-to-total ratio

### 1. Introduction

The combination of a bulge and a disk is a conventional model to represent the basic structure of galaxies. The variety of surface brightness profiles seen in galaxies is approximated reasonably well by assuming the  $r^{1/4}$ -law,

$$\log \frac{I_B(r)}{I_{e,B}} = -3.33 \left[ \left( \frac{r}{r_{e,B}} \right)^{1/4} - 1 \right], \quad (1)$$

---

<sup>1</sup>Present address: National Astronomical Observatory, Mitaka, Tokyo, 181-8588 Japan

for the bulge component and the exponential law,

$$\log \frac{I_D(r)}{I_{e,D}} = -0.729 \left[ \left( \frac{r}{r_{e,D}} \right) - 1 \right], \quad (2)$$

for the disk component. Here  $I_e$  is the effective surface brightness and  $r_e$  is the major-axis effective radius. The subscripts B and D denote bulge and disk, respectively. The effective surface brightness is usually expressed in units of mag arcsec<sup>-2</sup> as

$$\mu_e = -2.5 \log I_e. \quad (3)$$

The  $r^{1/4}$ -law was originally proposed to represent the profile of elliptical galaxies. These “laws” do not have firm physical basis (e.g., King 1978; Freeman 1970; Yoshii & Sommer-Larsen 1989; Makino, Akiyama, & Sugimoto 1990), and observed profiles of almost all galaxies show, to some degree, departures from these laws (e.g., Kormendy 1977a; Schombert & Bothun 1987; Shaw & Gilmore 1989). A number of authors (e.g., Kormendy & Bruzual 1978; Kent, Dame, & Fazio 1991; Andredakis et al. 1995; Courteau, de Jong, & Broeils 1996) have given evidence that many bulges can be fitted better by an exponential radial profile than by an  $r^{1/4}$ -law. Nevertheless, the empirical fitting functions (1) and (2) are useful for characterizing and deriving global properties of galaxies.

The distributions and mutual relationships of the scaling parameters,  $\mu_{e,B}$ ,  $r_{e,B}$ ,  $\mu_{e,D}$ , and  $r_{e,D}$ , are important clues to the investigation of formation and evolution of galaxies. Kormendy (1977a) found a tight correlation between  $\mu_e$  and  $r_e$  for elliptical galaxies. A similar but slightly different correlation holds for cD galaxies (Schombert 1987). Freeman (1970) was the first to point out a very small scatter of  $\mu_{e,D}$ , though he actually measured  $\mu_D(0)$  instead of  $\mu_{e,D}$  in his study, using a sample of 36 spiral and S0 galaxies. Disney (1976) and Allen & Shu (1979) claimed that the near constancy of  $\mu_{e,D}$  found by Freeman (1970) is a result of selection effects. Indeed, later studies found many fainter disks (e.g., van der Kruit 1987; Bothun et al. 1987; Impey, Bothun, & Malin 1988; Impey et al. 1996; Dalcanton et al. 1997), but brighter disks are rare (McGaugh 1996). The recent statistical study by de Jong (1996b) has shown the bivariate distribution functions including  $\mu_{e,D}$ , where we can see some kind of the Freeman’s law, but with a much larger scatter.

Our knowledge of the distributions and mutual relationships of the scaling parameters is, however, still insufficient. This is mainly because the samples analyzed so far are small and because the effects of various selection biases are not understood very well (e.g., Kent 1985; Kodaira, Watanabe, & Okamura 1986; Simien & de Vaucouleurs 1986; McGaugh 1996; de Jong 1996b; Dalcanton et al. 1997).

Most previous studies were based on the so-called profile decomposition technique, where the one-dimensional surface brightness profile is extracted from two-dimensional surface photometry and the bulge and the disk models are fit either iteratively or simultaneously (e.g., Kormendy 1977b; Boroson 1981; Kent 1985; Schombert & Bothun 1987). A few authors proposed a

two-dimensional image decomposition technique (Shaw & Gilmore 1989; de Jong 1996a). A method that depends on similar a priori fitting functions was also applied to the study of dark halo problem in spiral galaxies (e.g., Kent 1986; Athanassoula, E., Bosma, A., & Papaioannou, S. 1987). Such decomposition techniques, though they give relatively accurate parameters, require an image of a galaxy consisting of many pixels of high signal-to-noise ratio (hereafter S/N).

Images of a large number of faint galaxies are available now (e.g., Impey et al. 1996), and future CCD imaging surveys such as the Sloan Digital Sky Survey (hereafter SDSS; York 1998; Fukugita 1998) will increase the number by more than an order of magnitude. If we wish to understand the distributions and correlations of galaxy bulge and disk parameters and the implications of these distributions for galaxy formation and evolution, it is essential to derive parameters for these large samples and examine their statistical behavior, even if the determination for any individual galaxy is less accurate than could be obtained from a higher S/N image.

We show in this paper that the growth curve of galaxies is useful to this purpose. The growth curve is a plot of integrated magnitude as a function of the diameter of the integrating (circular) aperture. The growth curve is such a fundamental quantity that most future large imaging surveys will measure it for a large number of galaxies. The growth curve has been conventionally used to derive the asymptotic magnitude of galaxies by a method called growth curve fitting (e.g., de Vaucouleurs et al. 1976, RC2; de Vaucouleurs 1977; Kodaira et al. 1990, PANBG; de Vaucouleurs et al. 1991, RC3). We show that the growth curve can be used, in addition to this conventional purpose, to infer bulge and disk properties and bulge-to-total luminosity ratios of a large number of faint galaxies, if the point spread function (hereafter PSF) is accurately known and S/N is modest.

Since the original version of the present analysis was carried out in the course of performance verification of the photometric pipeline software of the SDSS, many parameters adopted in the present study are tuned for the SDSS. However, our conclusions are not subject to the particular choice of the parameters. We base our analysis on S/N, which is independent from the parameters of the observation, and give a cross reference figure between S/N and apparent magnitude that is valid for the SDSS.

We start in §2 with a description of simulated galaxy images on which the present analysis is largely based. The method of growth curve fitting and construction of template growth curves are described in §3. Results from the simulated data are summarized in §4. The effect of changing PSF is investigated in §5. Finally, a test of our method using images of real galaxies taken from PANBG is described in §6.

## 2. Simulated Galaxies

We use two samples of simulated galaxies originally constructed to investigate target selection criteria and photometric pipeline performance for the SDSS. The bright sample consists of 2110

galaxies with  $12 \lesssim r' \lesssim 18.5$  mag, while the faint sample includes 2199 galaxies with  $18.5 \lesssim r' \lesssim 23.3$  mag. The bright sample and the faint sample are relevant to the spectroscopic sample and the photometric sample of the SDSS, respectively. The SDSS  $r'$  band is centered at  $6230\text{\AA}$  with a full width at half maximum  $1370\text{\AA}$  (see Fukugita 1998)

Each simulated galaxy contains a bulge component and a disk component, though for elliptical galaxies the disk component has zero luminosity. The total  $B$ -band luminosities are drawn randomly from a Schechter (1976) luminosity function with parameters  $M_* = -19.68 + 5 \log h$  and  $\alpha = -1.07$ . Hubble types from E to Sc are randomly assigned. Bulge-to-disk luminosity ratios (in  $r'$ -band) are assigned as a function of Hubble type based on Kent (1985). K-corrected fluxes in the SDSS bandpasses are determined separately for the bulge and disk components using the fiducial galaxy spectral energy distributions of Coleman, Wu, & Weedman (1980). Disk scale lengths  $r_{e,D}$ , are set using the Freeman (1970) law and bulge scale lengths  $r_{e,B}$  using the fundamental plane relations as summarized by Maoz and Rix (1993), adjusted as a function of Hubble type based on Kent (1985). A Gaussian scatter of 0.15 rms in  $\log r_e$  is added in order to produce a range of surface brightness at each luminosity. Disk axis ratios are assigned assuming random inclinations, and bulge axis ratios are drawn randomly from the observed distribution tabulated by Ryden (1992). Galaxy positions in a 3-dimensional model universe are taken from a large, cold dark matter N-body simulation (by C. Park and J. R. Gott) in order to produce an appropriately clustered galaxy population, but for purposes of this paper each galaxy is analyzed in isolation and this clustering is unimportant. How to deal with 'blended images' is a separate problem, which we will not discuss in the present paper.

For each galaxy in the input catalog, we create a simulated image in which the bulge follows the  $r^{1/4}$ -law of equation (1) and the disk follows the exponential law of equation (2). Figure 1 shows the distribution of  $\log r_{e,B}$ ,  $\log r_{e,D}$ , and  $\eta = \log(r_{e,B}/r_{e,D})$  of our 4309 sample galaxies. Most galaxies have  $0''.1 \lesssim r_{e,B}, r_{e,D} \lesssim 10''$ .

Our two-dimensional galaxy images have the characteristics expected for the SDSS imaging survey; that is, we simulate a CCD observation made at the F/5 focus of a 2.5-m telescope in the  $r'$  band with a resolution of 0.4 arcsec/pixel and an exposure time of 55 seconds. Sky brightness is assumed to be  $21.2 \text{ mag arcsec}^{-2}$ . The CCD plus filter response is also simulated accordingly. Statistical photon noise is added to the image. The image is convolved with a double-Gaussian seeing profile,

$$I(r) = 0.9 \exp\left(-\frac{r^2}{2\sigma_1^2}\right) + 0.1 \exp\left(-\frac{r^2}{2\sigma_2^2}\right), \quad (4)$$

where we assume  $\sigma_1=0.376$  arcsec and  $\sigma_2=1.08$  arcsec to give a FWHM of  $w_s = 0.944$  arcsec.

We define the signal-to-noise ratio, S/N, of a galaxy as

$$S/N = \frac{\int [I(x, y) - I_{sky}] G dS}{[\int I(x, y) G dS]^{1/2}}, \quad (5)$$

where  $I(x, y)$  represents the counts in a pixel at  $(x, y)$  in the image,  $G$  is the gain factor, and

integration is made within a circular aperture of diameter 10 arcsec centered on the image. Figure 2 shows the S/N of 4309 galaxies as a function of apparent total magnitude  $m_{cat}$  taken from the input catalog.

### 3. Growth Curve Fitting and Template Growth Curves

#### 3.1. Method of Growth Curve Fitting

Growth curve fitting is a conventional method of galaxy photometry. A growth curve is defined by

$$\Delta m(\xi) = m(\xi) - m_{asym}, \quad (6)$$

and

$$\xi = \log \left( \frac{r}{r_e} \right), \quad (7)$$

where  $m(\xi)$  is the magnitude of a galaxy integrated in a *circular* aperture of radius  $r$ . The asymptotic magnitude is defined by

$$m_{asym} = m(\infty). \quad (8)$$

For the image of a galaxy with the center already identified, we measure the magnitude of the galaxy integrated in a series of circular apertures and obtain

$$\{m_i(\xi_i); i = 1, 2, \dots, N\}. \quad (9)$$

The template growth curves are fit to the series of measurements and the best-fit template is used to derive  $m_{asym}$ . The *effective radius*  $r_e$  is also obtained from the best-fit template as

$$\Delta m(0) = 0.75, \quad \log r = \log r_e. \quad (10)$$

Note that  $r_e$  derived in this way is the effective radius of the whole galaxy and not of an individual component. Note also that  $r_e$  is the *circular-aperture effective radius* and is different from the *major-axis effective radius* that would be obtained by model fitting to the major-axis profile.

If a set of templates has a reasonable resolution in the scaling parameters, we can retrieve the bulge and disk parameters from the best-fit template. It is rather difficult to construct such a set of growth curves based on real data. This is why we use model galaxies instead of real data to construct the set of growth curve templates, as described below.

#### 3.2. Template Growth Curves

The conventional method of growth curve fitting relies on template growth curves derived from real data. A template is usually made for each morphological type index (de Vaucouleurs

1977; RC2; RC3), and in some cases for different inclinations as well (PANBG). It is important that the templates cover the full range of galaxy profiles.

Here we adopt a rather new approach of constructing the templates using model galaxies that have a full range of realistic parameters. A model galaxy for the template consists of a bulge and a disk, which have the surface brightness distributions of equations (1) and (2), respectively. The templates used here are no longer the one-dimensional series of morphological type index as in the previous studies. We characterize the templates by two parameters. One is the bulge-to-total luminosity ratio  $B/T$ , and the other is the ratio of the effective radii  $\eta = \log(r_{e,D}/r_{e,B})$ .

Another important factor is the effect of seeing. Seeing has different influence on galaxies with different apparent sizes. In order to characterize the effect, we introduce another parameter

$$\zeta = \log(r_{e,D}/w_s), \quad (11)$$

where  $w_s$  is the FWHM of the PSF (the seeing profile). Assuming typical seeing of  $w_s \sim 1''$ , we take  $-1 < \log \zeta < 1$ , which is appropriate for galaxies concerned (see Figure 1).

The ranges and the bin sizes of these parameters for the present set of templates are summarized in Table 1. In total, 1089 ( $=11 \times 9 \times 11$ ) templates are created. Template growth curves are computed analytically for *face-on* inclination using equations (1) and (2). They are then convolved with the seeing profile of equation (4). Convolution is performed in two dimensions on the assumption of axisymmetry. Figure 3 shows the 99 template growth curves before convolution with the seeing profile.

### 3.3. Practical Procedure

In practice, for each galaxy, the sum of the squared residuals is computed for all the templates as

$$\delta^2 = \sum_{i=3}^N w_i \left[ m(\log r_i) - m_{asym} - \Delta m \left( \log \frac{r_i}{r_e}(l, m, n) \right) \right]^2 + \frac{1}{4} [\log r_e - \log r_e(l, m, n)]^2, \quad (12)$$

where  $w_i$  is the weight and  $(l, m, n)$  denotes the grid in the  $(B/T, \eta, \zeta)$  space. The second term of the right-hand side is incorporated to avoid an apparently ‘good’ fit by a template with a very different  $r_e$ . In the present study, we adopt the weight as

$$w_i = \log r_i. \quad (13)$$

For a given set of  $(l, m, n)$ , the best-fit values of  $m_{asym}$  and  $\log r_e$  are computed by minimizing  $\delta^2$ . The template that gives the smallest value of  $\delta^2$  is chosen as the best-fit template. We adopt the bulge and disk parameters of the best-fit template as our estimates of their values.

This fitting procedure itself does not care about what kinds of models are used to create the template. Our choice of the  $r^{1/4}$ -law for the bulge component is a convention. There is

growing evidence that many bulges have steeper surface brightness profiles than the  $r^{1/4}$ -law and that they are better fitted by exponential profiles. However, to examine the validity of these models is beyond the scope of the present analysis. We would have similar but slightly different parameters if we used exponential models for the bulge component, as demonstrated by, for example, Andredakis & Sanders (1994).

Table 2 shows the radii of our integrating apertures. We follow the common practice of dropping from the fitting procedure magnitudes that are integrated in a small aperture whose size is comparable to or smaller than the seeing scale. In the present study, the innermost two magnitudes are not used in the growth curve fitting (see equation (12)). Care should also be taken not to be affected badly by occasional erratic behavior of the outermost data points due to incorrect sky subtraction and/or excessive noise.

## 4. Results

### 4.1. Asymptotic Magnitude

In the measurement of  $m_i(\xi_i)$  for each of the simulated galaxies, we reject data that either have  $S/N < 1$  or  $m_i > m_{i-1}$ . As a result, 279 galaxies in the faint sample yield fewer than four usable values of  $m_i(\xi_i)$ , the minimum number required to derive the asymptotic magnitude with our scheme (equation 12). Ten of these galaxies have three data values, 16 have two, six have one, and 247 have none. Accordingly, asymptotic magnitudes are not determined for the 279 galaxies. These galaxies are very faint and/or very small.

Figure 4(a) shows the magnitude difference

$$\delta m = m_{asym} - m_{cat}, \quad (14)$$

as a function of  $m_{cat}$ , where  $m_{cat}$  is the total magnitude given in the input catalog, i.e., the correct answer. Figure 4(b) shows the magnitude difference as a function of  $S/N$ . It is seen in Figure 4(b) that  $\delta m(\text{rms}) \lesssim 0.1$  for  $S/N \gtrsim 30$  ( $\log S/N \sim 1.5$ ). We hereafter take  $S/N=30$  as the boundary between high- $S/N$  galaxies and low- $S/N$  galaxies.

In the case of some of the lowest- $S/N$  galaxies ( $S/N \lesssim 5$ ), the best-fit template gives an asymptotic magnitude that is very different from the true value ( $>2$  mag). A typical example is shown in Figure 5. If one wishes to pursue this method to such low- $S/N$  galaxies at the cost of relatively large error in the resulting asymptotic magnitude, one could impose some constraint in order to circumvent the problem, for example, that

$$m_{asym} - m_{cat} > -2, \quad (15)$$

when searching the best-fit template. However,  $m_{cat}$  is, of course, not available in the analysis of real data. We can replace  $m_{cat}$  with an isophotal magnitude in this case.

## 4.2. Bulge-to-Total Luminosity Ratio

Figure 6(a) shows the correlation between the input and output (measured)  $B/T$  for high-S/N galaxies. The input (catalog)  $B/T$  values are sorted into 10 bins of width  $\Delta(B/T) = 0.1$ , and for each of the 10 bins the histogram of the output  $B/T$  values is shown in the separate panels by the solid line.

There is a reasonably good correlation between the input and output values. This is promising because it suggests that we can estimate  $B/T$  by growth curve fitting for galaxies with high S/N. In the panels of high- $B/T$  bins ( $B/T > 0.5$ ), the histograms show weak tails extending to low  $B/T$  values. The tail can be seen even in the highest bin ( $B/T = 1$ ). An inspection reveals that the tail mostly consists of galaxies that have small bulges with  $r_{e,B} \lesssim 1$  pixel (0.4 arcsec). In the panels of low- $B/T$  bins ( $B/T < 0.2$ ), on the other hand, tails are also seen to extend toward large  $B/T$  values. This tail mostly consists of highly inclined galaxies with  $b/a \lesssim 0.2$ , which are very rare in reality. In fact, only 264 (1.2%) and 2043 (9.5%) out of 21611 galaxies in RC3 catalog have  $b/a < 0.1$  and  $b/a < 0.2$ , respectively.

It is reasonable that we cannot retrieve  $B/T$  either for high- $B/T$  (bulge-dominated) galaxies with small  $r_{e,B}$  or for low- $B/T$  (disk-dominated) galaxies with a highly inclined disk. In fact, if we restrict our sample to galaxies with  $S/N > 30$  and  $[(B/T > 0.5 \text{ and } r_{e,B} > 1) \text{ or } (B/T < 0.5 \text{ and } (b/a)_D > 0.2)]$ , we obtain a much tighter correlation, as shown by the solid line in Figure 6(b). However, it is impossible, of course, to restrict a sample of observed galaxies according to their *intrinsic* parameters. Figure 6(b) is just to show that our method works properly.

On the other hand, there is almost no correlation for low-S/N galaxies (Figure 6(c)). This suggests that little information on  $B/T$ , and hence on bulge and disk parameters, can be retrieved for galaxies with  $S/N \lesssim 30$ .

The correlation shown in Figure 6(a) is promising for use in coarse morphological (structural) classification of galaxies. In order to investigate quantitatively the use of the output  $B/T$  for the morphological classification, we present the statistics in Table 3, where the correlation matrix between output  $B/T$  and input  $B/T$  is given for five classifications based on  $B/T$  for four S/N classes. The mean and the standard deviation of input  $B/T$  ( $\mu_i, \sigma_i$ ) and those of output  $B/T$  ( $\mu_o, \sigma_o$ ) are also given. The former values,  $\mu_i$  and  $\sigma_i$  are determined by the input sample and do not have much significance. We define the true fraction by  $N_{true}/N_m$ , where  $N_{true}$  is the number of galaxies that are correctly measured in a given output  $B/T$  bin and  $N_m$  is the number of all galaxies in the bin. We compute the true fraction in two ways; for  $\Delta(B/T) = \pm 0.1$  we count only the galaxies in the same output  $B/T$  bin as the input  $B/T$  bin while for  $\Delta(B/T) = \pm 0.3$  the difference of  $\pm 1$  bin is allowed for. The latter case,  $\Delta(B/T) = \pm 0.3$ , may correspond to three coarse classifications as 'early', 'intermediate', and 'late', according to  $B/T$ .

It is remarkable that the true fraction for  $\Delta(B/T) = \pm 0.3$  is as high as  $\gtrsim 80\%$  in  $S/N > 30$  and that it does not change very much as a function of S/N. However, the true fraction is significantly

lower in  $30 > S/N > 10$ . In the SDSS,  $S/N \sim 30$  corresponds to  $r' \sim 19$  mag (Figure 2). The number of galaxies observed in the SDSS brighter than this magnitude will be of the order of  $10^6$ . It is very important to obtain even coarse classification for such a large number of galaxies, and the method of growth curve fitting is a promising tool for this purpose.

Figure 7 shows the mean of output  $B/T$  ( $\mu_o$ ) as a function of the mean of input  $B/T$  ( $\mu_i$ ) for the four S/N classes. The error bars, which are shown only for the highest and the lowest S/N classes for clarity, represent the standard deviations,  $\sigma_o$  and  $\sigma_i$ . These values are taken from Table 3. The three high S/N classes ( $S/N > 30$ ) show similar correlations between  $\mu_o$  and  $\mu_i$ . There is a systematic trend that  $B/T$  is overestimated for  $B/T(\text{input}) \lesssim 0.5$  but underestimated for  $B/T(\text{input}) \gtrsim 0.7$ . This trend is due to the extended tails noted above. The correlation for the lowest S/N class ( $S/N < 30$ ) is, however, considerably different, showing a larger degree of degradation in the output  $B/T$ . This marked change of behavior is the reason we have chosen  $S/N=30$  as the boundary between high-S/N and low-S/N galaxies.

### 4.3. Bulge and Disk Parameters

Figure 8 shows the correlations between the input and output values for  $r_{e,B}$  and  $r_{e,D}$ . For  $r_{e,B}$ , only the galaxies with  $B/T > 0.2$  are plotted, while for  $r_{e,D}$ , only those with  $B/T < 0.8$  are plotted. The filled circles and small dots are for face-on galaxies ( $(b/a)_B \geq 0.8$  and  $(b/a)_D \geq 0.8$ ) and inclined galaxies ( $(b/a)_B < 0.8$  or  $(b/a)_D < 0.8$ ), respectively. Left panels are for high-S/N galaxies and right panels for low-S/N galaxies.

Low-S/N galaxies show almost no correlation, as expected from the  $B/T$  statistics. However, high-S/N galaxies show reasonably tight correlations. It is seen that  $r_{e,B} \sim 1$  pixel (0.4 arcsec;  $\log r_{e,B} \sim -0.4$ ) is the limit below which we cannot retrieve the bulge parameters, as expected from the analysis of  $B/T$ . Statistics are shown in Table 4 in the similar format to Table 3.

Face-on galaxies, which should have better match with the templates, show fairly good correlations. However, it is interesting to see that most of the inclined galaxies also show correlations that are only slightly poorer than those of face-on galaxies. This indicates that growth curve fitting is not very sensitive to galaxy inclination.

## 5. Effect of Changing PSF

It is natural that the retrieval of  $B/T$  and the bulge/disk parameters from the best-fit template is sensitive to the shape of the PSF. We investigate this effect by applying an artificially changed PSF to the templates while keeping the true PSF applied to the simulated galaxies. Considering the practical application, here we restrict ourselves to a slight change of the PSF between the templates and the data, which would easily result from errors in the construction of

the PSF. A much larger difference in the PSF shape would clearly jeopardize the analysis, but it is reasonable to assume that with good imaging data the PSF will be known to good, but not perfect, accuracy.

The PSF is usually constructed by summing up stellar images in a CCD frame by the shift and add method. Such a PSF may well show a slight departure from the true PSF due to image deterioration. We created a large number of simulated (noisy) images of a 21 mag star. We intentionally chose among them four images that have smaller FWHM than the average and reconstructed the PSF using the four by a conventional shift-and-add method. The resulting PSF is slightly but systematically different from the true (noiseless) PSF. The reconstructed PSF has a FWHM of 0.919 arcsec while the true PSF has FWHM of 0.944 arcsec. The two PSFs and their profile difference are shown in Figure 9. The profile difference is less than 30% in the core of the PSF but amounts to  $\gtrsim 50\%$  in the envelope. However, their difference in the FWHM is only 2.6%.

The histogram of  $B/T$  obtained with this reconstructed PSF is shown for high-S/N galaxies in Figures 6(a)-6(c) by the broken line. We find only a little difference. Accordingly,  $B/T$  statistics of such galaxies are shown to be insensitive to change of the PSF at a few % level in FWHM. Correlations between the input and output values for bulge and disk parameters also show only a slight change.

## 6. A Test using Real Images of Bright Galaxies

As a test on real data, we apply the technique to images of nearby galaxies taken from PANBG. There are 103 galaxies in PANBG whose  $B/D$  ratios are measured by Kodaira et al. (1986), where  $B/D$  is the bulge-to-disk luminosity ratio and  $B/T = (1 - 1/(1 + B/D))$ . The magnitudes of these galaxies are  $m_B=9-12$  mag. Their images, which are digitized images of Schmidt plates, usually include more than  $10^4$  pixels above the detection threshold. The seeing FWHM of these data is 1–4 pixels, which is negligibly small compared with the size of the galaxies.

We measure their images in the same manner as the simulated images. Figure 10 shows the comparison of the  $B/T$ . There is a reasonably good correlation between the two completely independent measurements. Most measurements agree with each other within  $\Delta(B/T) = \pm 0.1$ . Figure 11 shows our  $B/T$  as a function of the morphological type index. There is also a reasonably good correlation. The scatter between  $B/T$  and type index is substantial, but most previous investigations also show similar scatter (e.g., Kodaira, Watanabe, & Okamura 1986; Andredakis and Sanders 1994; de Jong 1996b).

## 7. Conclusion and Discussion

We have shown that the growth curve of galaxies is useful for determining bulge and disk parameters and bulge-to-total luminosity ratios in addition to conventional asymptotic magnitudes. Simulated images of 4309 galaxies with a wide range of bulge and disk parameters are created. Template growth curves are constructed from model galaxies that cover the full range of realistic bulge and disk parameters. The effect of seeing is also modeled in the growth curve templates.

We find that the bulge-to-total luminosity ratio and bulge and disk parameters are reasonably well retrieved, in addition to the conventional asymptotic magnitude (rms error  $\lesssim 0.1$  mag), for galaxies with  $S/N \gtrsim 30$ , if the error of PSF is  $\lesssim$  a few percents in FWHM. A coarse, three-bin  $B/T$  classification can be made at a confidence level of more than 80 percent for galaxies with  $S/N \gtrsim 30$ .

Finally, it should be noted that the present analysis gives rather optimistic estimates for the accuracy of this method for two reasons. First, our simulated images and the template growth curves are constructed from the same series of models, consisting of an  $r^{1/4}$ -law bulge and an exponential disk. Real galaxies often show slight departures from the model as noted already. Such departures may well introduce some error in the estimate of the parameters. However, the growth curve is not sensitive to such slight departures because it is an integrated profile, so template mismatch should not be a severe problem at least in the case of regular galaxies. Second, envelopes of bright stars sometimes overlap on faint galaxies in the actual survey data. They make sky subtraction difficult and introduce systematic error, which is difficult to quantify accurately. Both of these potential difficulties will have to be investigated in the context of individual large imaging data sets, such as the SDSS. However, the success of our tests here suggests that growth curve fitting will be a valuable tool in the analysis of such data sets, aiding the passage from pixel data to statistical characterization and physical understanding of the galaxy population.

We thank M.Doi, Y.Komiyama, and W.Kawasaki for useful discussion on many subjects related to this paper. We thank Michael Strauss for assistance in calculating the K-corrected fluxes for the artificial galaxy catalog and Changbom Park and Richard Gott for contributing the N-body simulation used to construct this catalog. Special thanks go to the anonymous referee, who made many valuable comments that led to significant improvements of the manuscript. This work was supported in part by Grants-in-Aid (07CE2002, 09640312) from the Ministry of Education, Science, Sports, and Culture of Japan.

## REFERENCES

- Allen, R. J., & Shu, F. H. 1979, *ApJ*, 227, 67
- Andredakis, Y. C., & Sanders, R. H. 1994, *MNRAS*, 267, 283
- Andredakis, Y. C., Peletier, R. F., & Balcells, M. 1995, *MNRAS*, 275, 874
- Athanassoula, E., Bosma, A., & Papaioannou, S. 1987, *A&A*, 179, 23
- Boroson, T. 1981, *ApJS*, 46, 177
- Bothun, G. D., Impey, C. D., Malin, D. F., & Mould, J. R. 1987, *AJ*, 94, 23
- Coleman, G. D., Wu, C.-C., & Weedman, D. W. 1980, *ApJS*, 43, 393
- Cpurteau, S., de Jong, R. S., & Broeils, A. H. 1996, *ApJ*, 457, L73
- Dalcanton, J. J., Spergel, D. N., Gunn, J. E., Smith, M., & Schneider, D. P. 1997, *AJ*, 114, 635
- de Jong, R. S. 1996a, *A&AS*, 118, 557
- de Jong, R. S. 1996b, *A&A*, 313, 45
- de Vaucouleurs, G. 1977, *ApJS*, 33, 211
- de Vaucouleurs, G., de Vaucouleurs, A. & Corwin, H. G. 1976, *The Second Reference Catalogue of Bright Galaxies*, Austin: Univ. Texas Press (RC2)
- de Vaucouleurs, G., de Vaucouleurs, A., Corwin, H. G., Buta, R. J., Paturel, G., & Fouqué, P. 1991, *Third Reference Catalogue of Bright Galaxies*, New York: Springer (RC3)
- Disney, M. J. 1976, *Nature*, 263, 573
- Freeman, K. C. 1970, *ApJ*, 160, 811
- Fukugita, M. 1998, *Highlights of Astronomy* (in press)
- Impey, C. D., Bothun, G. D., & Malin, D. F. 1988, *ApJ*, 330, 634
- Impey, C. D., Sprayberry, D., Irwin, M. J., & Bothun, G. D. 1996, *ApJS*, 105, 209
- Kent, S. M. 1985, *ApJS*, 59, 115
- Kent, S. M. 1986, *AJ*, 91, 1301
- Kent, S. M., Dame, T.M., & Fazio, G. 1991, *ApJ*378, 131
- King, I. R. 1978, *ApJ*, 222, 1
- Kodaira, K., Watanabe, M., & Okamura, S. 1986, *ApJS*, 62, 703
- Kodaira, K., Okamura, S, & Ichikawa, S. 1990, *Photometric Atlas of Northern Bright Galaxies*, Tokyo: Univ. Tokyo Press (PANBG)
- Kormendy, J. 1977a, *ApJ*, 218, 333
- Kormendy, J. 1977b, *ApJ*, 217, 406
- Kormendy, J., & Bruzual A., G. 1978, *ApJ*, 223, L63

- Makino, J., Akiyama, K. & Sugimoto, D. 1990, PASJ, 42, 205  
Maoz, D., & Rix, H.-W. 1993, ApJ, 416, 425  
McGaugh, S. S. 1996, MNRAS, 280, 337  
Ryden, B. S. 1992, ApJ, 396, 445  
Schechter, P. 1976, ApJ, 203, 297  
Schombert, J. M. 1987, ApJS, 64, 643  
Schombert, J. M., & Bothun, G. D. 1987, AJ, 93, 60  
Shaw, M. A., & Gilmore, G. 1989, MNRAS, 237, 903  
Simien, F., & de Vaucouleurs, G. 1986, ApJ, 302, 564  
van der Kruit, P. C. 1987, A&A, 173, 59  
York, D. G. 1998, IAU Symp., 183 (in press)  
Yoshii, Y., & Sommer-Larsen, J. 1989, MNRAS, 236, 779

Table 1. Parameters for the template growth curves.

Parameter	range	bin size	number of templates
$B/T$	0.0 - 1.0	0.1	11
$\eta = \log(r_{e,B}/r_{e,D})$	-1.0 - 0.6	0.2	9
$\zeta = \log(r_{e,D}/w_s)$	-1.0 - 1.0	0.2	11

Table 2. Radii of the integrating aperture.

$i$	0	1	2	3	4	5	6	7
$r_i(\text{pix})$	0.56	1.69	2.58	4.41	7.51	11.58	18.58	28.55
$r_i(\text{''})$	0.224	0.676	1.032	1.764	3.004	4.632	7.432	11.42
$i$	8	9	10	11	12	13	14	
	45.50	70.51	110.5	172.5	269.5	420.5	657.5	
	18.2	28.2	44.2	69.0	107.8	168.2	263.0	

Table 3. Morphological classification based on  $B/T$  ratio.

output $B/T$	$N_m$	input $B/T$					True Fraction		
		0.0-0.2	0.2-0.4	0.4-0.6	0.6-0.8	0.8-1.0			
(S/N>200)		$\mu_i$	0.12	0.30	0.50	0.70	0.98	$\Delta(B/T)$	
		$\sigma_i$	0.06	0.05	0.06	0.06	0.06	( $\pm 0.1$ )	( $\pm 0.3$ )
0.0-0.2	27		18	9	0	0	0	67%	100%
0.2-0.4	62		16	30	14	2	0	48%	97%
0.4-0.6	132		11	29	58	31	3	44%	89%
0.6-0.8	125		2	6	26	71	20	57%	94%
0.8-1.0	53		0	1	1	5	46	87%	96%
total	399	$\mu_o$	0.33	0.45	0.58	0.69	0.87		
		$\sigma_o$	0.17	0.16	0.13	0.10	0.10		
(200>S/N>100)		$\mu_i$	0.10	0.30	0.50	0.71	0.98	$\Delta(B/T)$	
		$\sigma_i$	0.05	0.06	0.06	0.06	0.06	( $\pm 0.1$ )	( $\pm 0.3$ )
0.0-0.2	71		50	16	2	1	2	70%	93%
0.2-0.4	175		60	64	30	18	3	37%	88%
0.4-0.6	271		25	62	90	75	19	33%	84%
0.6-0.8	171		6	16	22	98	29	57%	87%
0.8-1.0	70		1	1	1	10	57	81%	96%
total	758	$\mu_o$	0.34	0.46	0.53	0.65	0.79		
		$\sigma_o$	0.17	0.16	0.12	0.14	0.19		
(100>S/N>30)		$\mu_i$	0.10	0.28	0.49	0.70	0.99	$\Delta(B/T)$	
		$\sigma_i$	0.06	0.06	0.06	0.06	0.05	( $\pm 0.1$ )	( $\pm 0.3$ )
0.0-0.2	143		102	23	5	10	3	71%	87%
0.2-0.4	265		89	100	43	31	2	38%	88%
0.4-0.6	351		59	78	102	93	19	29%	78%
0.6-0.8	256		13	14	39	118	72	46%	89%
0.8-1.0	61		0	1	2	9	49	80%	95%
total	1076	$\mu_o$	0.33	0.43	0.54	0.61	0.78		
		$\sigma_o$	0.18	0.15	0.15	0.16	0.16		
(30>S/N>10)		$\mu_i$	0.10	0.31	0.51	0.71	0.99	$\Delta(B/T)$	
		$\sigma_i$	0.06	0.05	0.07	0.05	0.04	( $\pm 0.1$ )	( $\pm 0.3$ )
0.0-0.2	42		12	6	4	16	4	29%	43%
0.2-0.4	55		5	6	3	26	15	11%	25%
0.4-0.6	90		8	6	6	40	30	7%	58%
0.6-0.8	72		8	1	4	28	31	39%	88%
0.8-1.0	11		0	0	0	2	9	82%	100%
total	270	$\mu_o$	0.40	0.39	0.47	0.51	0.60		
		$\sigma_o$	0.27	0.20	0.21	0.21	0.20		

Table 4a. Correlation statistics for the bulge scale length.

output log $r_{e,B}$	$N_m$	input log $r_{e,B}$					
		-3.0 - -1.0	-1.0 - -0.5	-0.5 - 0.0	0.0 - 0.5	0.5 - 1.6	
(S/N>200)		$\mu_i$	-1.49	-0.67	-0.22	0.27	0.80
		$\sigma_i$	0.37	0.12	0.13	0.13	0.23
-3.0 - -1.0	0		0	0	0	0	0
-1.0 - -0.5	1		0	1	0	0	0
-0.5 - 0.0	71		1	4	43	22	1
0.0 - 0.5	154		2	4	11	123	14
0.5 - 1.6	173		4	0	6	15	148
total	399	$\mu_o$	0.48	-0.02	0.01	0.29	0.79
		$\sigma_o$	0.41	0.36	0.29	0.18	0.28
(200>S/N>100)		$\mu_i$	-1.37	-0.67	-0.21	0.26	0.73
		$\sigma_i$	0.27	0.13	0.14	0.14	0.18
-3.0 - -1.0	4		0	4	0	0	0
-1.0 - -0.5	16		1	6	9	0	0
-0.5 - 0.0	209		1	26	120	62	0
0.0 - 0.5	290		2	17	47	195	29
0.5 - 1.6	239		9	9	30	65	126
total	758	$\mu_o$	0.74	-0.01	0.05	0.29	0.69
		$\sigma_o$	0.67	0.50	0.36	0.26	0.23
(100>S/N>30)		$\mu_i$	-1.61	-0.69	-0.23	0.25	0.71
		$\sigma_i$	0.50	0.14	0.14	0.14	0.16
-3.0 - -1.0	10		1	8	1	0	0
-1.0 - -0.5	19		1	7	10	1	0
-0.5 - 0.0	266		8	45	130	82	1
0.0 - 0.5	380		10	22	93	215	40
0.5 - 1.6	401		20	18	54	138	171
total	1076	$\mu_o$	0.43	-0.03	0.15	0.35	0.71
		$\sigma_o$	0.54	0.52	0.38	0.29	0.25
(30>S/N>10)		$\mu_i$	-1.21	-0.70	-0.24	0.18	0.67
		$\sigma_i$	0.23	0.12	0.14	0.13	0.19
-3.0 - -1.0	14		2	11	1	0	0
-1.0 - -0.5	32		4	15	10	3	0
-0.5 - 0.0	130		7	18	77	26	2
0.0 - 0.5	73		1	12	26	32	2
0.5 - 1.6	21		2	1	2	11	5
total	270	$\mu_o$	-0.23	-0.38	-0.13	0.18	0.53
		$\sigma_o$	0.57	0.50	0.34	0.33	0.49

Table 4b. Correlation statistics for the disk scale length.

output log $r_{e,D}$	$N_m$	input $\log r_{e,D}$				
		-1.0 - -0.5	-0.5 - 0.0	0.0 - 0.5	0.5 - 1.6	
(S/N>200)		$\mu_i$	-0.58	-0.15	0.31	0.69
		$\sigma_i$	0.08	0.12	0.12	0.18
-1.0 - -0.5	1		0	0	1	0
-0.5 - 0.0	75		2	24	49	0
0.0 - 0.5	215		0	0	163	52
0.5 - 1.6	108		0	6	3	99
total	399	$\mu_o$	-0.10	-0.02	0.22	0.58
		$\sigma_o$	0.10	0.46	0.19	0.19
(200>S/N>100)		$\mu_i$	-0.52	-0.20	0.29	0.66
		$\sigma_i$	0.02	0.13	0.13	0.15
-1.0 - -0.5	4		0	4	0	0
-0.5 - 0.0	188		2	54	132	0
0.0 - 0.5	385		0	4	297	84
0.5 - 1.6	181		0	20	10	151
total	758	$\mu_o$	-0.00	0.11	0.19	0.57
		$\sigma_o$	0.00	0.48	0.20	0.17
(100>S/N>30)		$\mu_i$	-0.61	-0.20	0.29	0.68
		$\sigma_i$	0.10	0.13	0.14	0.16
-1.0 - -0.5	10		0	10	0	0
-0.5 - 0.0	279		21	83	175	0
0.0 - 0.5	496		1	15	351	129
0.5 - 1.6	289		0	51	27	211
total	1074	$\mu_o$	-0.05	0.20	0.21	0.58
		$\sigma_o$	0.10	0.54	0.22	0.18
(30>S/N>10)		$\mu_i$	-0.63	-0.24	0.16	0.61
		$\sigma_i$	0.09	0.13	0.12	0.07
-1.0 - -0.5	9		0	9	0	0
-0.5 - 0.0	117		29	66	21	1
0.0 - 0.5	21		0	7	13	1
0.5 - 1.6	72		0	63	9	0
total	219	$\mu_o$	-0.04	0.27	0.23	0.20
		$\sigma_o$	0.08	0.58	0.40	0.20

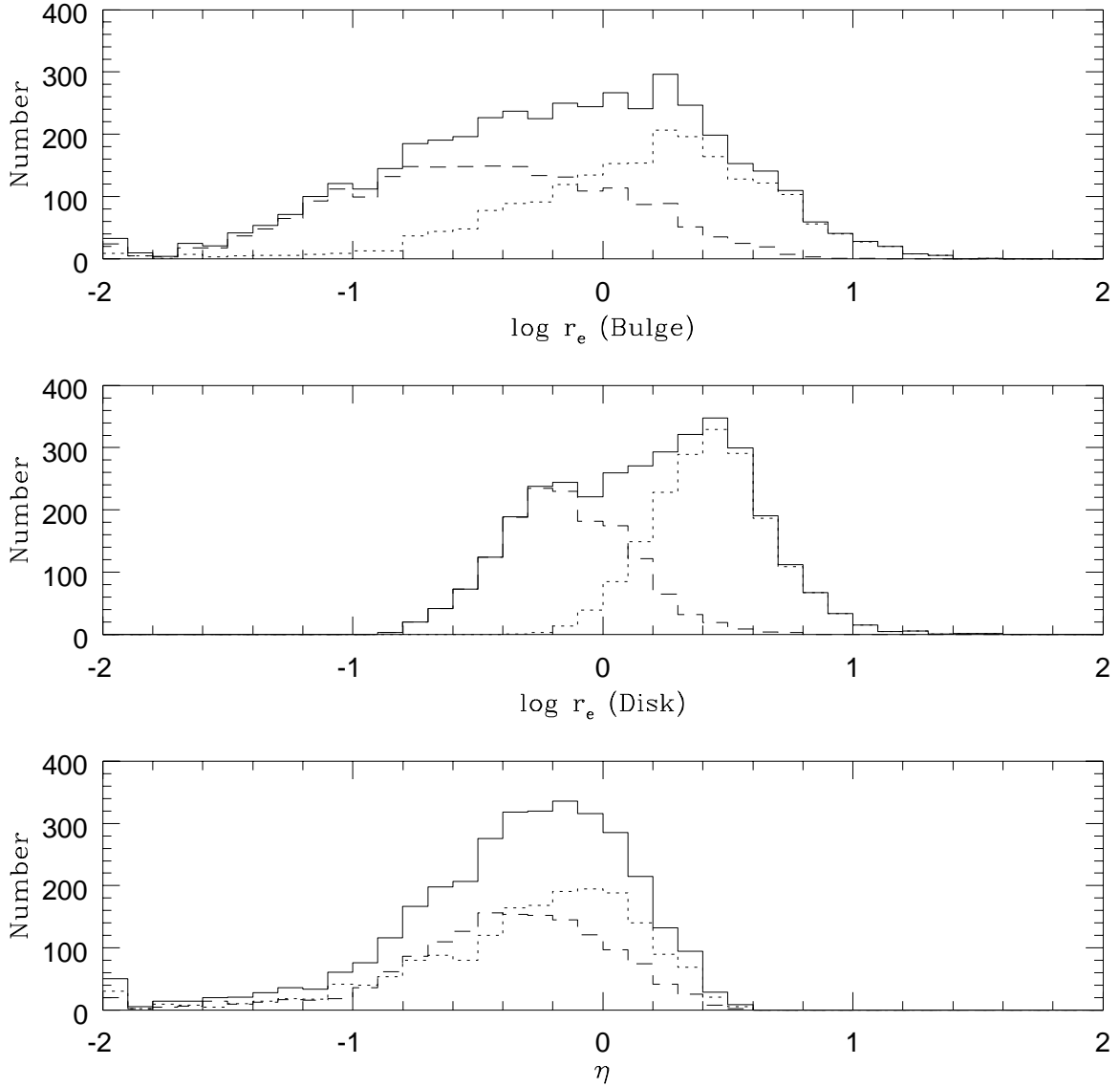


Fig. 1.— Histograms of  $\log r_{e,B}$  (top),  $\log r_{e,D}$  (middle), and  $\eta = \log(r_{e,B}/r_{e,D})$  of our sample galaxies. Units are in arcsec. The solid line shows the total 4309 galaxies, while the dotted line and the broken line are for 2110 galaxies in the bright sample and for 2199 galaxies in the faint sample, respectively.

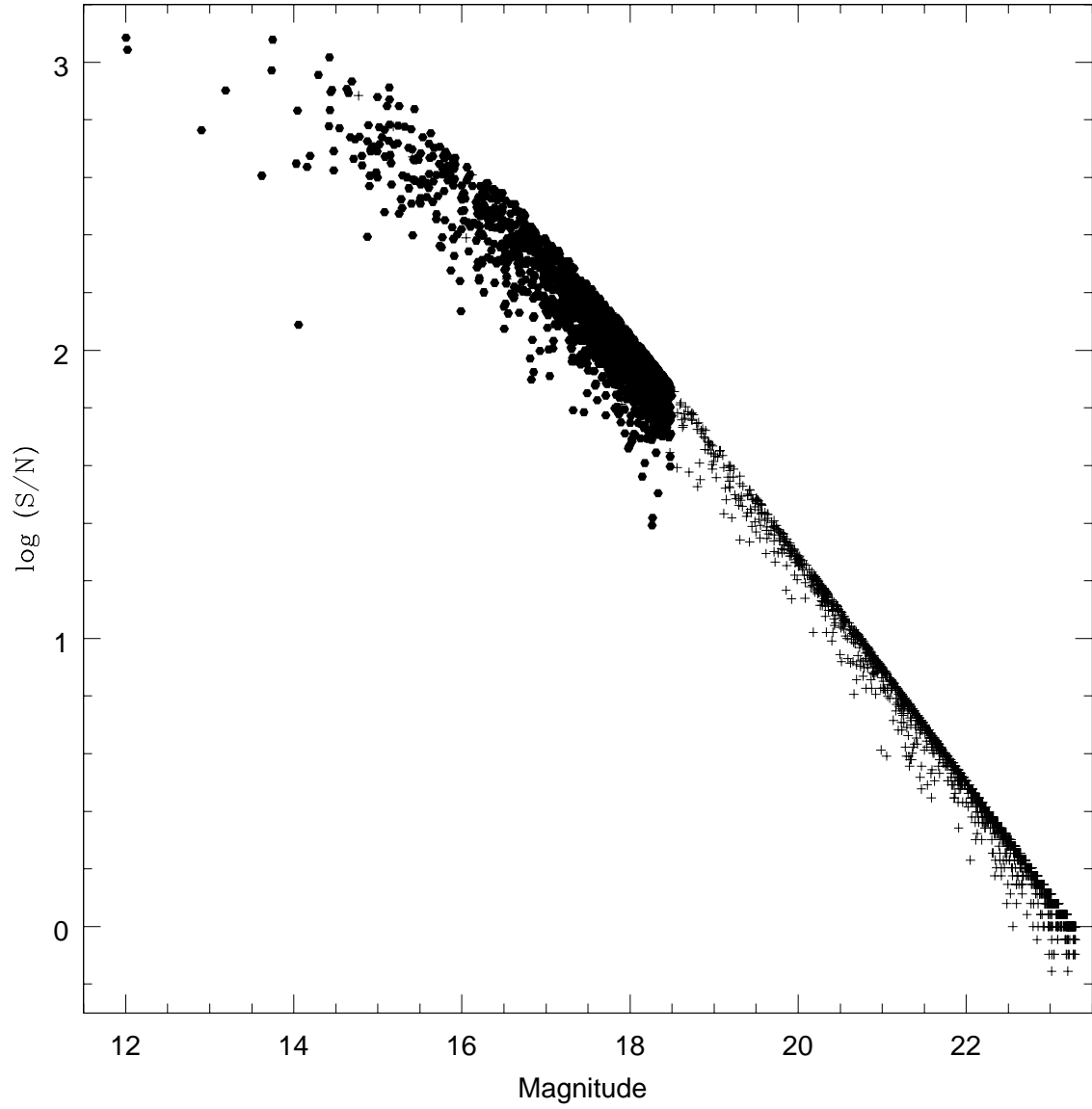


Fig. 2.— Signal-to-noise ratio of the 4309 simulated galaxies as a function of apparent total magnitude taken from the input catalog. Filled circles are galaxies in the bright sample and pluses are those in the faint sample.

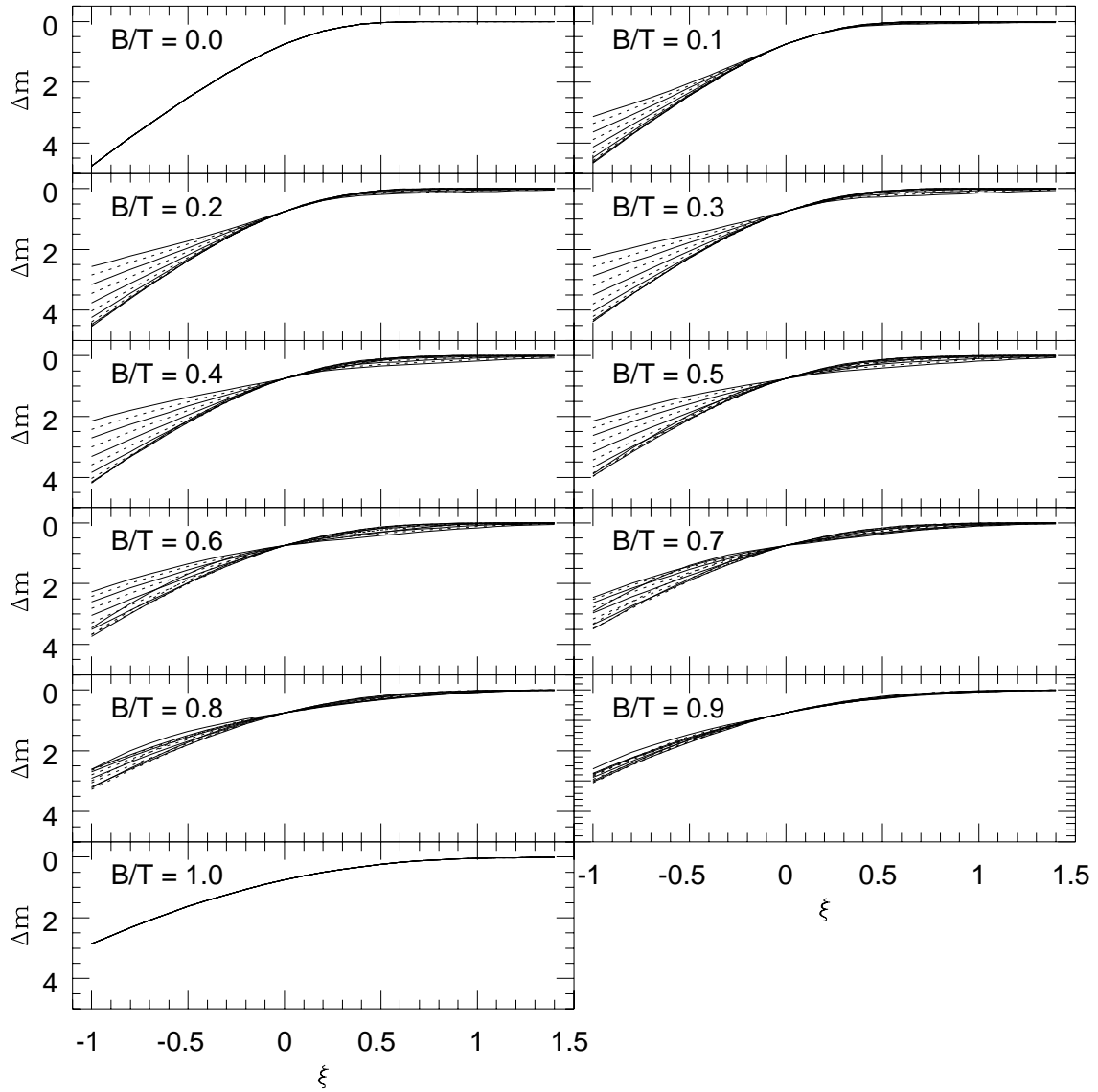


Fig. 3.— Template growth curves before convolution with the seeing profile.

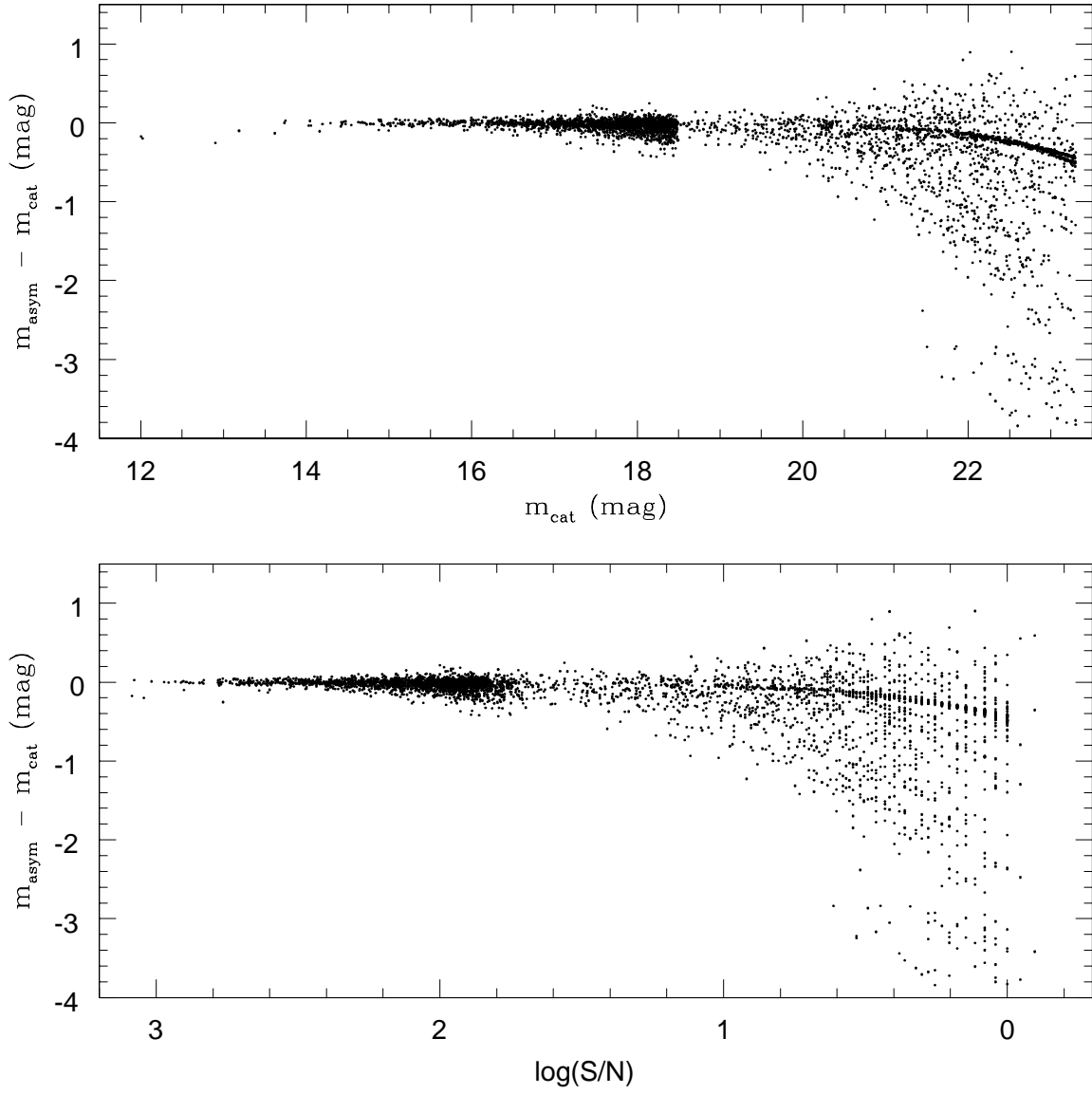


Fig. 4.— Magnitude difference,  $\Delta m = m_{\text{asym}} - m_{\text{cat}}$ , as a function of  $m_{\text{cat}}$  (a) and of S/N (b).

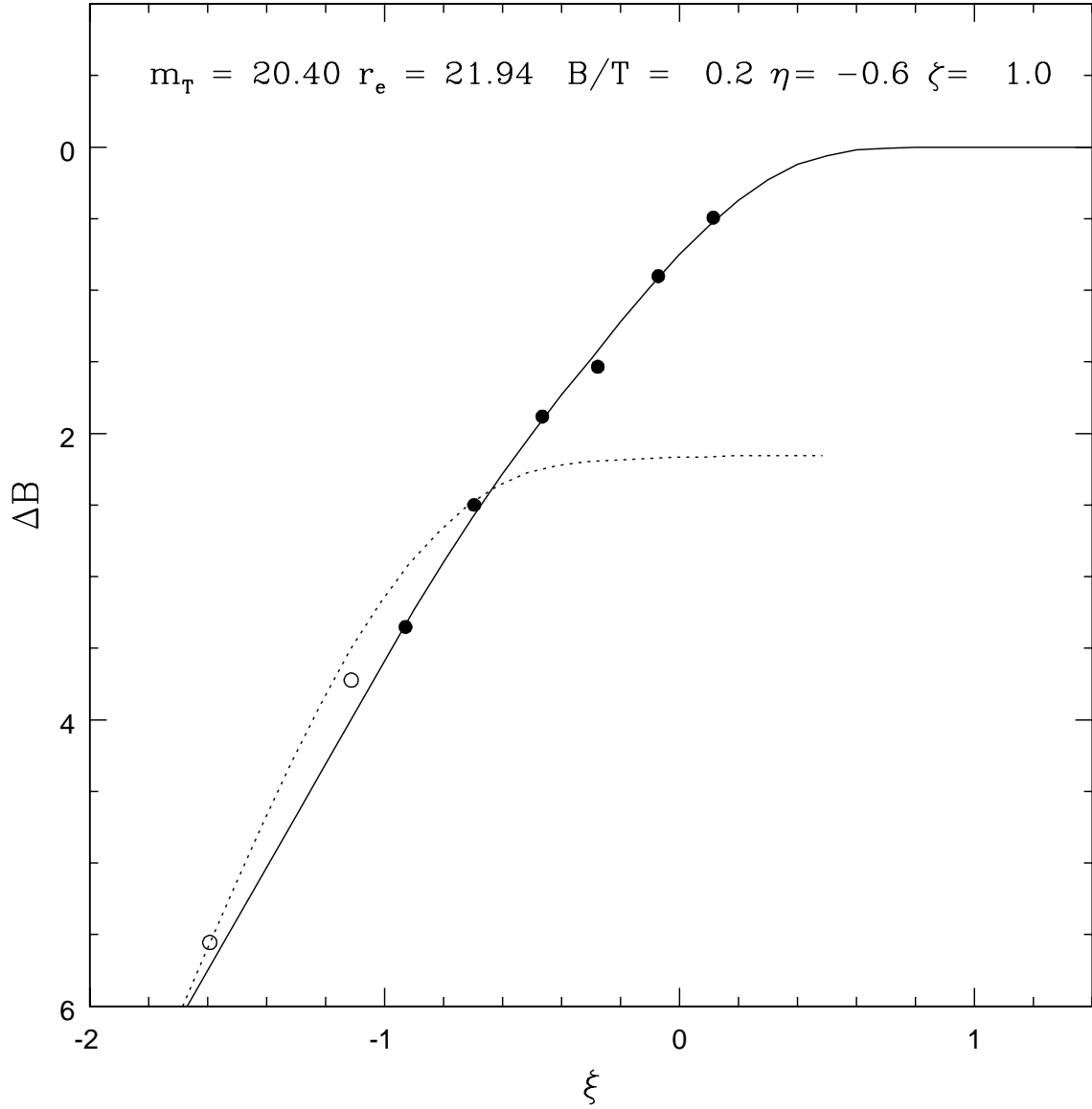


Fig. 5.— An example of wrong fit for a low-S/N galaxy. The dotted curve is the growth curve of the input noiseless image. Open and filled circles are measurements obtained from the simulated noisy image. The solid curve is the best fit template (Two open circles are not used in the fit). Outer measurements are seen to be largely affected by noise (mostly due to incorrect background subtraction)

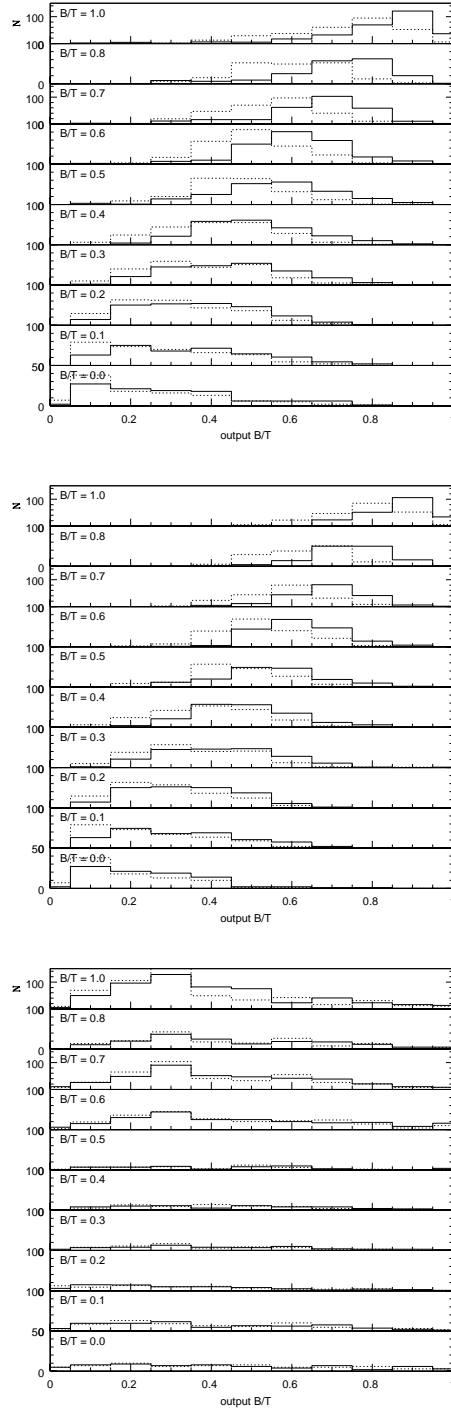


Fig. 6.— The correlation between the input and output  $B/T$  ratios for all high-S/N galaxies (a), galaxies with  $S/N > 30$  and  $[(B/T > 0.5 \text{ and } r_{e,B} > 1) \text{ or } (B/T < 0.5 \text{ and } (b/a)_D > 0.2)]$ (b), and low-S/N galaxies (c). The input (catalog)  $B/T$  values are sorted into 10 bins of width  $\Delta(B/T) = 0.1$ , and for each of the 10 bins, the histogram of the output  $B/T$  values are shown in the separate panels. Solid lines show the result with the true noiseless PSF while broken lines are for artificially changed PSF (see the text and Figure 9).

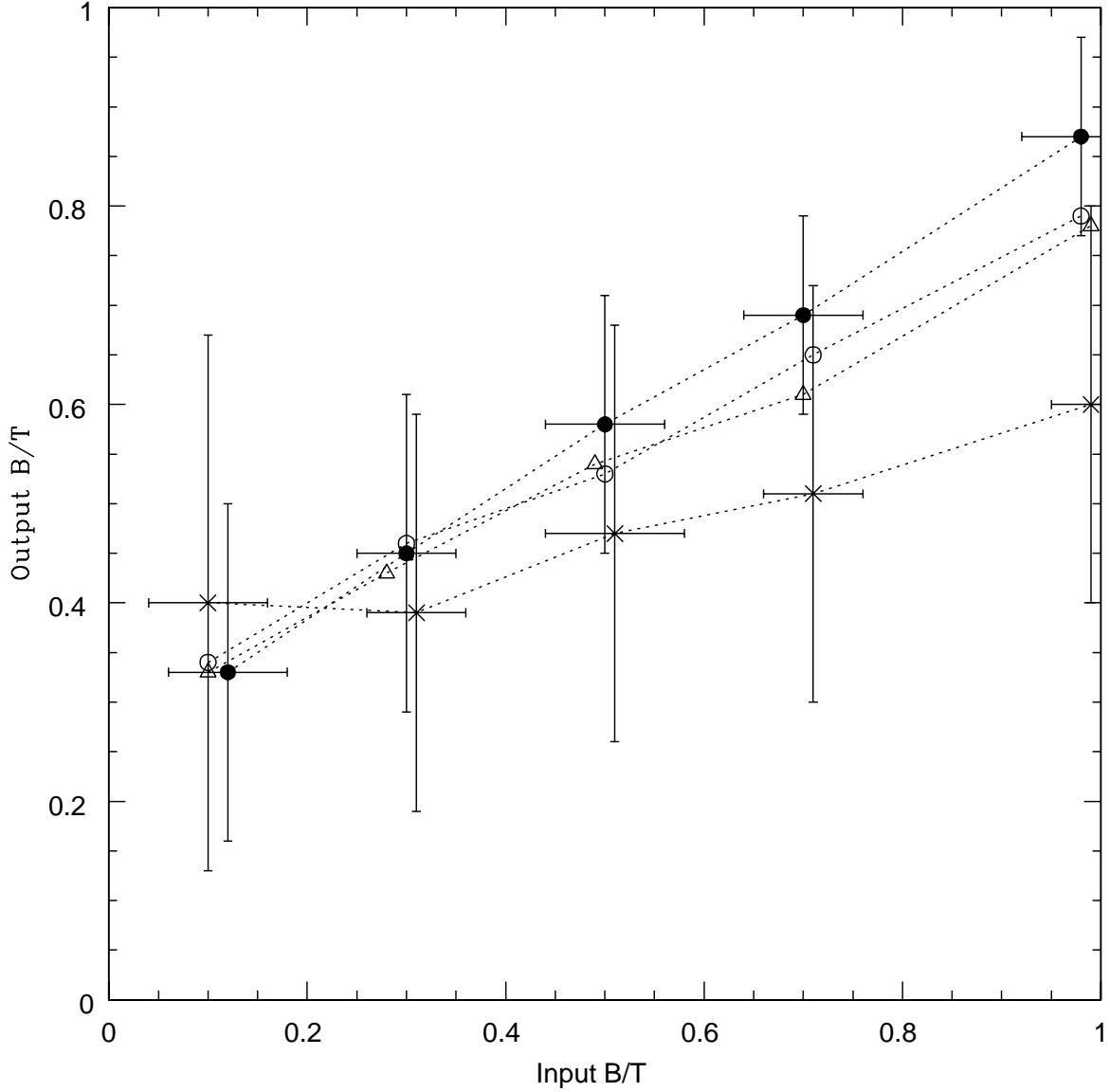


Fig. 7.— The mean of measured  $B/T$  as a function of the mean of input  $B/T$  for the four S/N classes. The error bars, which are shown only for the highest and the lowest S/N classes for clarity, represent the standard deviation. These values are taken from Table 3. Filled circles, open circles, open triangles, and crosses are for  $S/N > 200$ ,  $200 > S/N > 100$ ,  $100 > S/N > 30$ , and  $30 > S/N > 10$ , respectively.

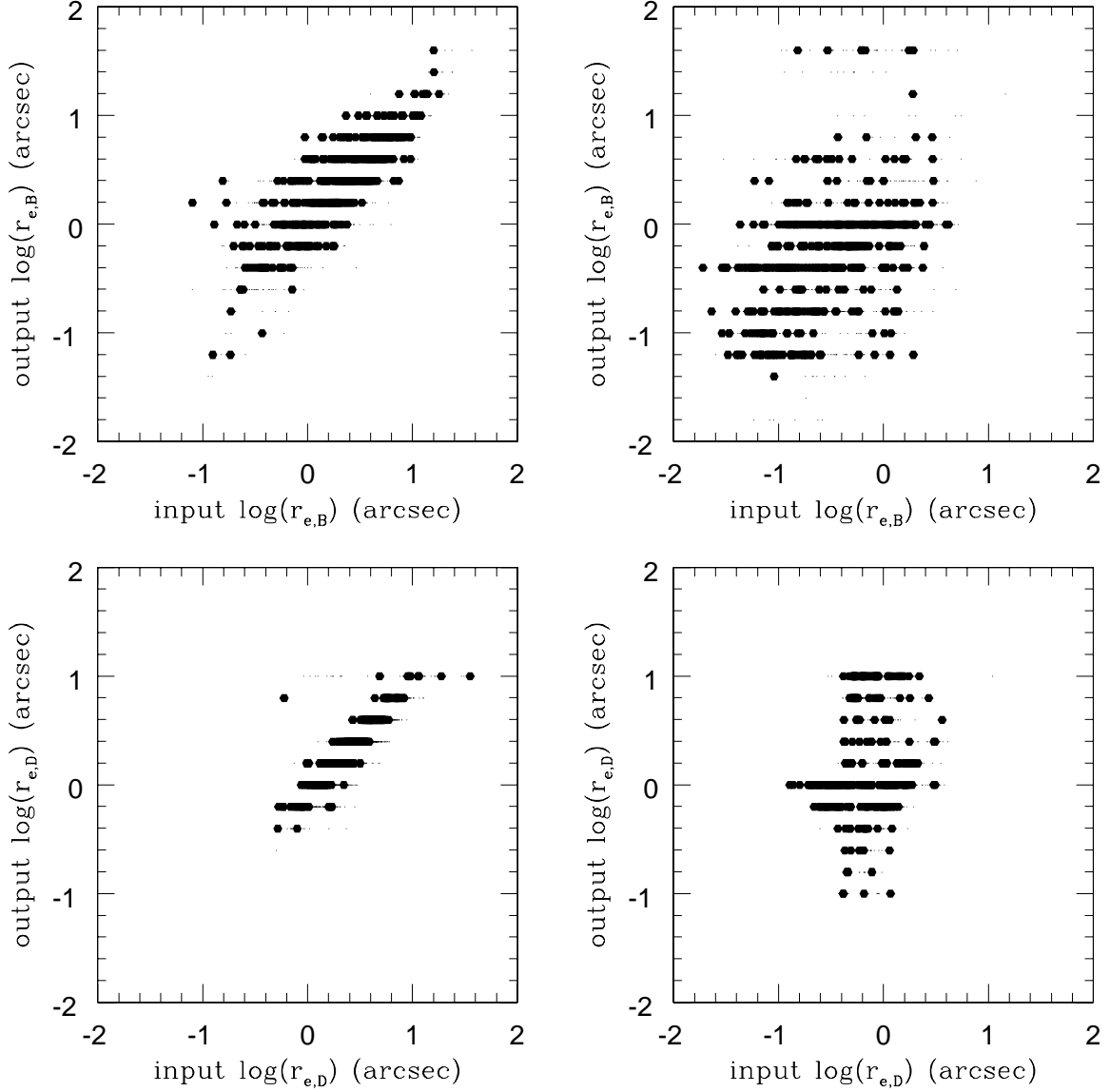


Fig. 8.— The correlations between the input and output values for  $r_{e,B}$  (upper panels; only for those with  $B/T > 0.2$ ) and  $r_{e,D}$  (lower panels; only for those with  $B/T < 0.8$ ). Left panels are for high-S/N galaxies and the right panels are for low-S/N galaxies. Filled circles are for face-on ( $(b/a)_B \geq 0.8$  and  $(b/a)_D \geq 0.8$ ) galaxies and small dots are inclined ( $(b/a)_B < 0.8$  or  $(b/a)_D < 0.8$ ) galaxies.

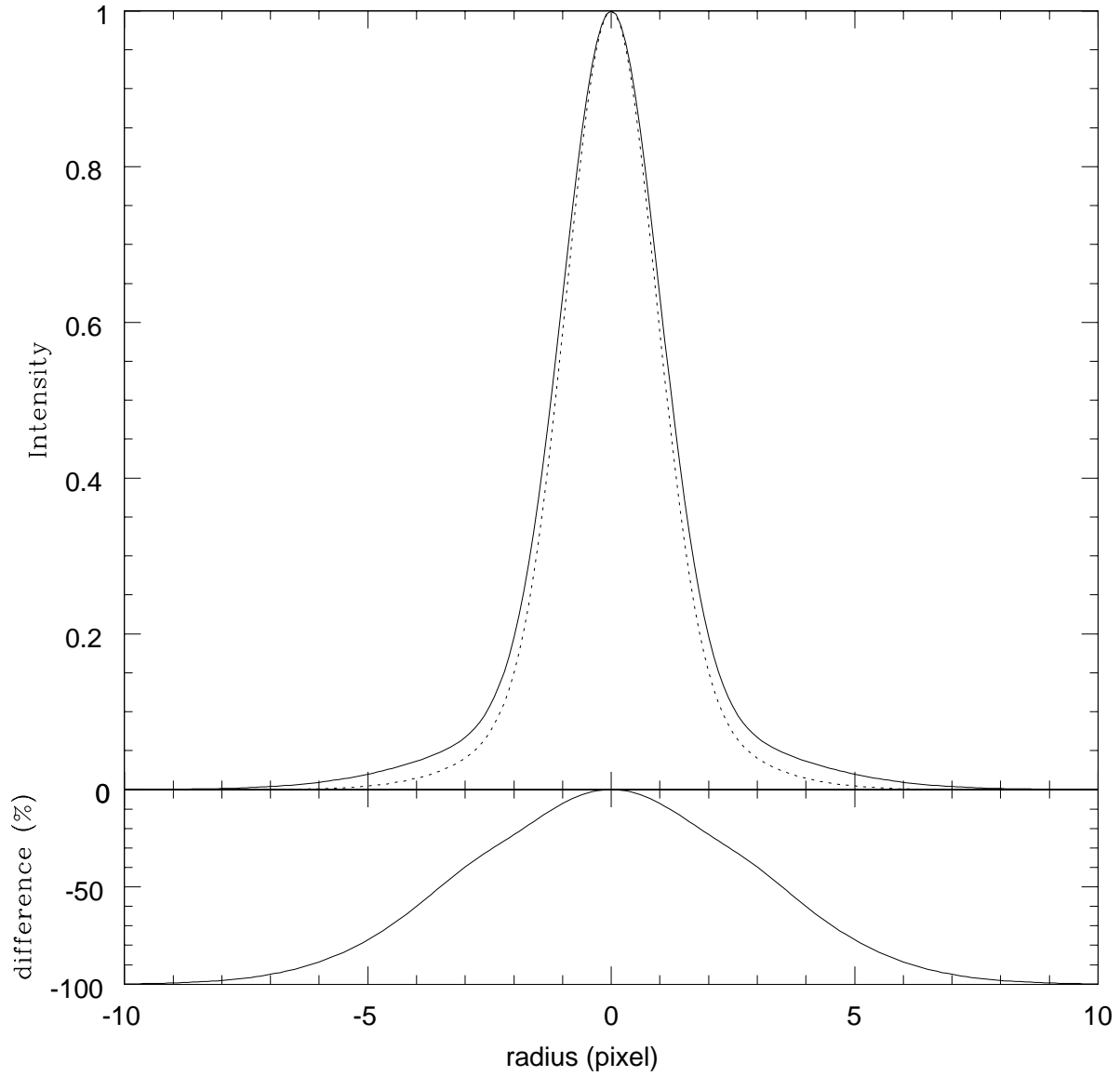


Fig. 9.— Upper panel shows the true noiseless PSF (solid line) compared with the PSF reconstructed from four simulated noisy images of a 21 mag star (broken line) (see the text). Lower panel shows the difference,  $(\text{PSF}(\text{true}) - \text{PSF}(\text{rec.})) / \text{PSF}(\text{true})$ .

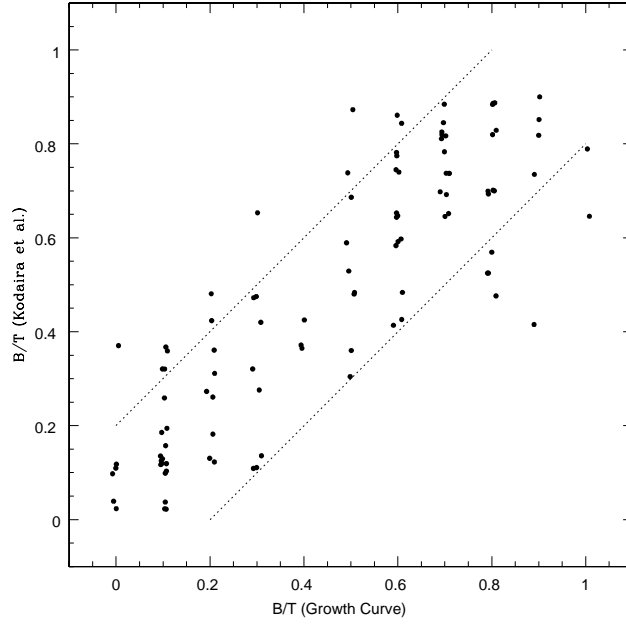


Fig. 10.— Comparison of  $B/T$  between Kodaira et al. (1986) and present study. Broken line show  $\Delta(B/T) = \pm 0.1$ .

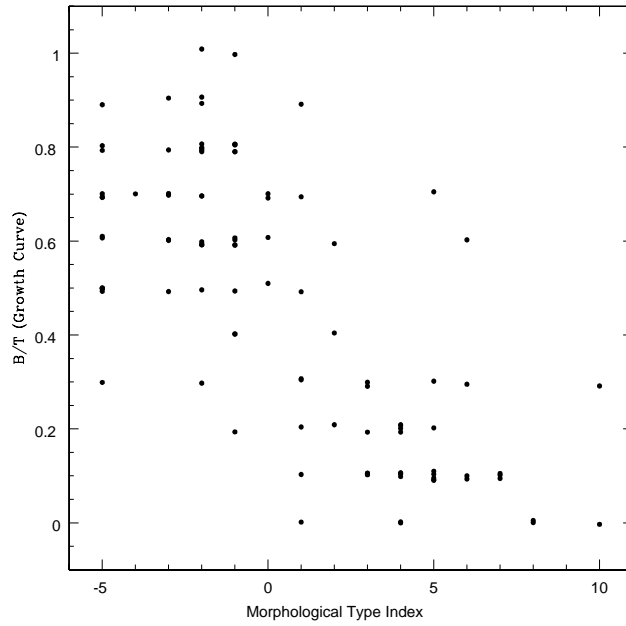


Fig. 11.—  $B/T$  obtained by the present method as a function of the morphological type index